ANALYSIS OF VIBRATION CHARACTERISTICS AND STRUCTURAL OPTIMIZATION OF THE CHASSIS FRAME OF CRAWLER-TYPE COMBINE HARVESTER
/
履带式联合收割机底盘机架振动特性分析与结构优化

Zihao ZHAO[1)], Chengqian JIN[12)], Guangyue ZHANG[2)], Youliang NI[2)], Zhenjie QIAN[2)]
[1)] School of Agricultural Engineering and Food Science, Shandong University of Technology, Zibo, Shandong / China
[2)] Nanjing Institute of Agricultural Mechanization, Ministry of Agriculture and Rural Affairs, Nanjing, Jiangsu / China
Corresponding author: Chengqian JIN
Tel: +8615366092900; E-mail: jinchengqian@caas.cn
DOI: https://doi.org/10.35633/inmateh-75-14

Keywords: *vibration characteristics; chassis; static analysis; vibration velocity*

ABSTRACT
To investigate the vibration characteristics of the Thinker Agricultural Machinery 4LZ-2.0 crawler-type combine harvester under operational conditions, vibration tests were conducted on the chassis frame at three different engine speeds: 2700 r/min, 1500 r/min, and 800 r/min. A static analysis was initially performed to identify regions of significant stress and deformation on the chassis frame, which guided the placement of measurement points for collecting vibration acceleration data. Subsequent processing of the acceleration data in the frequency domain revealed the variation in vibration velocity at each measurement point on the chassis frame. It was found that as the engine speed increased, the excitation frequencies from the vibrating screen and cutting platform appeared as dominant resonance frequencies at nine out of twelve measurement points on the chassis frame. By referencing the international standard ISO 20816, it was determined that most of these measurement points fell into Class D, indicating a high level of vibration severity. To mitigate the vibration of the chassis frame, two measures were implemented: enhancing the structural rigidity of the frame and reducing the area of the center of mass trajectory of the vibrating screen. Following these modifications, re-testing showed that the average vibration intensity at the three maximum vibration measurement points of the chassis in the high engine speed condition successfully decreased by 34.57% compared to the original structure.

摘要
为了解收割机运行状态下底盘机架振动特性，以星光农机 4LZ-2.0 型履带式联合收割机为研究对象，在发动机处于 2700r/min,1500r/min,850r/min 三种不同转速下对其底盘机架进行振动测试。首先通过静力分析找到底盘机架应力与变形较大的区域，并以此在其表面布置测点，采集振动加速度数据。通过在频域内对加速度数据进行处理得到底盘机架各测点振动速度变化情况。发现随发动机转速提升，振动筛与割台的激励频率在收割机底盘机架 12 个测点中 9 个测点作为主振频率出现。结合国际标准 ISO 20816，发现这些测点大多处于振动等级最大的 D 级，振动强度过大。为减小收割机底盘机架振动，采取增强机架结构、减小振动筛质心运动轨迹面积两种措施。经重新测试，发动机高转速状态下底盘 3 个振动最大测点各方向平均振动强度较原结构成功降低 34.57%。

INTRODUCTION
The chassis is the primary load-bearing component of a tracked combine harvester, subject to complex external excitations. Variations in the working environment and the machine's operational state can significantly affect its vibration characteristics, leading to considerable discrepancies in vibrational responses. Excessive vibrations not only impact the comfort of the operator (*Biriș et al., 2022; Vlăduţ et al., 2023; Dimitriadis et al., 2023; Marin et al., 2024*) but also increase the risk of fatigue failure at structurally weak points, thereby posing a serious threat to the overall reliability of the machine *(Zhou et al., 2023; Noh et al., 2024)*. Consequently, it is crucial to investigate the vibrational characteristics of the combine harvester chassis.

Currently, research on the vibrations of harvesters, both domestically and internationally, primarily focuses on the cutting platform, chassis, and operator comfort *(Ma et al., 2020; Jiang et al., 2017; Sun et al., 2014; Xie et al., 2019)*. Various methodologies, including dynamic simulation and analysis, experimental modal analysis, and test rig design, have been employed to obtain the vibrational characteristics of these components. *Wang et al. (2021)* designed an intelligent control test bench for combine harvesters, which is capable of regulating the forward speed of the combine harvester based on data processing results. Additionally, the system can classify and handle faults, as well as transmit and print stored data via serial communication. This design not only enhances the intelligence level of combine harvesters but also provides reliable technical support for fault diagnosis and performance optimization. By integrating data processing and automatic control functions, the test bench serves as a significant experimental platform and research foundation for the intelligent development of agricultural machinery. Comparing the results of the different methods for vibration and sound datasets, *Karagiovanidis et al.* (2023) found that classification accuracy showed that in the case of vibration, the detection of cavitation in real conditions is possible. *Rabbani et al.* (2011) constructed a dynamic three-dimensional model for a half-track tractor, incorporating its bounce, pitch, and roll motions, to elucidate the tractor's vibration characteristics. Driving experiments were conducted to validate the effectiveness of the motion equations derived from the proposed dynamic model. *Pang et al. (2019)* measured and analyzed the time-domain and frequency-domain characteristics of the cutting platform's vibrational response, designing a rubber-sleeved nut that successfully reduced the vibrations transmitted to the operator's seat. *Chen et al. (2020)* assembled the combine harvester's chassis and threshing frame into a complete structure, deriving its vibrational response under multi-source excitations to provide a reference for further improvements to the chassis. *Tang et al. (2021)* conducted finite element modal analysis and vibration testing on the threshing cylinder and frame, designing support beams based on test results to mitigate vibrations generated during the threshing process.

In summary, the vibration characteristics of agricultural machinery systems have garnered considerable attention from numerous scholars *(Yao et al., 2017; Li et al., 2023; Ding et al., 2022; Zhang et al., 2023)*. However, analyses regarding the impact of the engine, vibrating screen, and cutting mechanism on the chassis of tracked combine harvesters during operational conditions remain limited. This study primarily employs digital signal processing, complemented by finite element analysis and multi-body dynamic simulation, to explore this issue further.

MATERIAL AND METHODS

SOURCES OF CHASSIS FRAME VIRBATION AND INTRODUCTION TO CHASSIS STRUCTURE

The study focuses on the 4LZ-2.0 tracked combine harvester produced by Xingguang Agricultural Machinery, with its chassis frame primarily subjected to excitations from the engine, cutting platform, threshing drum, vibrating screen, and screw conveyor *(Zhang et al., 2021; Gao et al., 2017; Zhang et al., 2001)*. The spatial distribution of these components is illustrated in Figure 1.

Research on the excitatory conditions affecting the chassis is based on its structural design, as depicted in Figure 2. The chassis measures 2.75 m in length, 1.87 m in width, and 0.6 m in height. Constructed from carbon structural steel, the components are connected via welding. The orange section represents the chassis frame, with a steel pipe cross-section parameter of 40 × 60 × 3 mm. This frame directly connects to the engine, elevator, threshing drum, vibrating screen assembly, cutting platform, and the hydraulic support rods for the conveyor trough, while being anchored to two longitudinal beams (blue structure) that play a major load-bearing role.

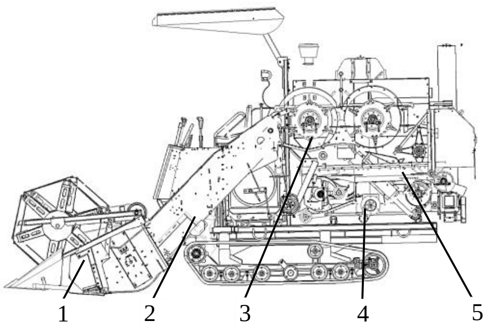

Fig. 1 - Sources of excitation for the chassis frame
1.Cutter bar; 2. Conveying trough; 3. Threshing drum; 4. Auger; 5. Vibrating screen

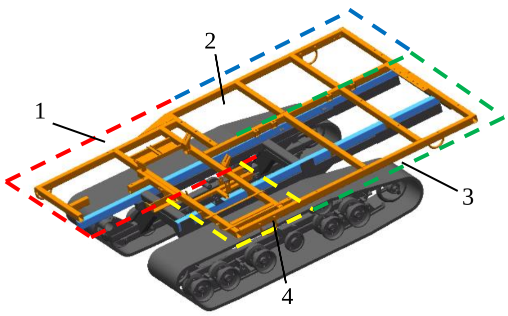

Fig. 2 - The chassis structure of the 4LZ-2.0 crawler-type combine harvester
1. Engine and cab area; 2. Grain bin area; 3. Threshing drum and vibrating screen area; 4. Cutter bar and conveying trough area

The longitudinal beams utilize steel pipes with a cross-section parameter of 50 × 70 × 3 mm, welded and fixed in place by two transverse beams with a cross-section parameter of 70 × 70 × 3 mm. These transverse beams are strategically located beneath the chassis frame at the front and middle sections, with each transverse beam linked to a truss structure. The loads borne by the chassis frame are transmitted through the truss to the track bearing wheel assembly, ultimately transferring the forces to the ground.

The structural simplification of the chassis model for the 4LZ-2.0 tracked combine harvester involves removing through-holes with diameters less than 10 mm and fillets with radii less than 5 mm, which have minimal impact on structural strength. Small flat surfaces are merged before importing the model into the finite element analysis software Ansys for static analysis. To enhance computational efficiency, the track components are excluded, and the track bearing wheel assembly is fixed as a boundary condition.

The connection methods between structures utilize the software's default settings, with structural steel selected as the material. The element size is set to 10 mm, resulting in a total of 1111691 nodes and 387396 elements. Based on manufacturer-provided parameters, the total mass of the machine is 2870 kg, with the chassis mass being 1318 kg. A vertical load of 15520 N is applied downward on the chassis frame's upper plane to simulate its stress condition in a static state, allowing for the calculation of total deformation and equivalent stress, as shown in Figure 3.

The static analysis results indicate that the chassis frame experiences the maximum deformation in the regions of the vibrating screen and threshing drum, which are farthest from the truss support. The grain tank area exhibits the next highest deformation. Stress and strain concentrations are most significant near the support points, highlighting these areas as relatively weak points in the overall frame that warrant close attention.

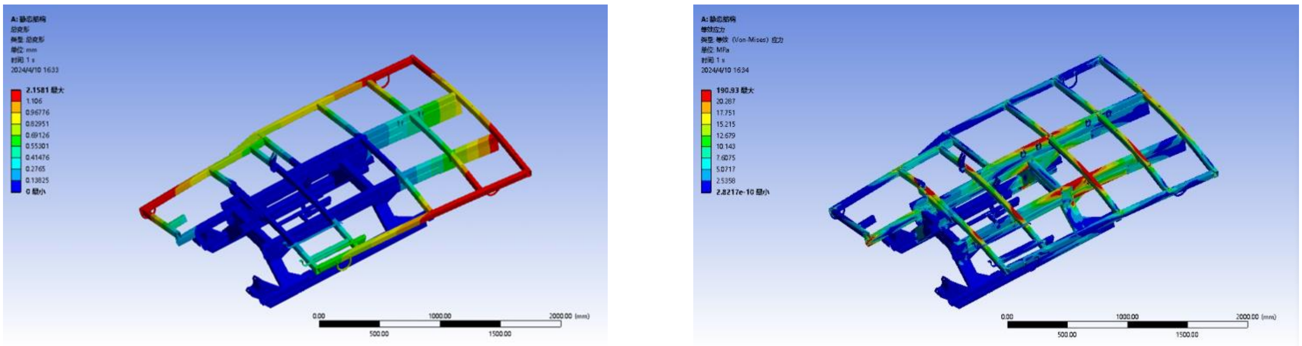

(a)Total deformation (b)von Mises stress

Fig. 3 - The static analysis results of the chassis

TESTING OF CHASSIS VIBRATION CHARACTERISTICS

The current international standard ISO 20816 provides guidelines for evaluating mechanical vibrations on non-rotating components based on the root mean square (RMS) vibration velocity. Vibrational intensity is categorized into four levels—A, B, C, and D—ranging from low to high. Given the differing operational characteristics of various types of machinery, the boundaries for each level are presented as fuzzy intervals, allowing users to make determinations based on their specific contexts. The boundary intervals are detailed in Table 1. In this study, each vibration level is defined by its maximum value as the boundary. Due to the large size of vibration velocity sensors, which makes them impractical for installation on the harvester chassis, vibration data is collected using acceleration sensors. This data is subsequently integrated to obtain the vibration velocity.

Vibration testing of the entire machine and the chassis frame was conducted using the Donghua Testing DH5902 data acquisition and analysis system, along with a portable computer and 12 tri-axial piezoelectric accelerometers (1A314E). This accelerometer captures acceleration amplitudes in the mutually orthogonal x, y, and z directions, with a measurement range of 500 $m \cdot s^2$ and a frequency acquisition range of 0.5 to 7000 Hz, set at a sampling frequency of 1000 Hz.

In conjunction with the static analysis results, 12 measurement points were selected on the chassis frame, evenly distributed across areas of significant deformation or stress, as shown in Figure 4. Measurement points 1, 2, 8, and 10 are located in the regions of the vibrating screen and threshing drum, points 3, 4, 5, and 11 in the grain tank area, points 6 and 12 near the engine, and points 7 and 9 in the cutting platform and conveyor trough areas.

Table 1

Boundary Intervals of Vibration Levels

AB Boundary / mm•s^{-1}	BC Boundary / mm•s^{-1}	CD Boundary / mm•s^{-1}
0.71-4.5	1.8-9.3	4.5-14.7

Table 2

The Vibration Frequencies of the Main Excitation Sources of the Harvester at Different Engine Speeds

Excitation source	Main excitation frequency /Hz		
	Low speed	Medium speed	High speed
Engine	28.33	50.00	90.00
Cutter drive shaft	2.83	5.00	9.00
Vibrating screen	2.37	4.17	7.50
Threshing drum	7.08	12.50	22.50
Screw conveyor	1.01	1.79	3.21

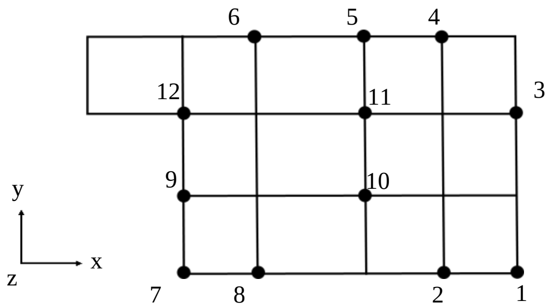

Fig. 4 - Distribution of measurement points

The vibration acceleration information in the x, y, and z directions was collected at various engine speeds: low (850 r/min), medium (1500 r/min), and high (2700 r/min). The time-domain information was analyzed, and the primary excitation frequencies associated with each source at different engine speeds are summarized in Table 2. The main excitation frequency of the engine is primarily determined by its second-order ignition frequency (*Wu, et al., 2020; Hu, et al., 2015*), The main vibration frequency f is calculated using the formula:

$$f = \frac{n}{60} \times \frac{c}{2} \tag{1}$$

where: n is the engine speed in revolutions per minute (r/min),

- c is the number of cylinders in the engine.

This formula provides the primary excitation frequency related to the engine's operational characteristics.

Fig. 5 – Tri-axial piezoelectric accelerometers (1A314E) at measurement point-2

Fig. 6 - Complete machine vibration testing

RESULTS

Calculation of Vibration Velocity at Each Measurement Point

To obtain the vibration velocity at each measurement point on the combine harvester chassis, the collected vibration acceleration data must be integrated. However, the velocity data obtained from direct time-domain integration is significantly affected by factors such as zero drift of the accelerometer and disturbances from other low-frequency signals, leading to noticeable trends in the results, as illustrated in Figure 6.

To eliminate these influences, it is necessary to fit the integration results and remove the trend components. However, fitting each group of signal data during large-scale signal processing can consume significant computational resources. Additionally, filtering out low-frequency components from the signal can also achieve a similar effect to detrending after integration (*Wei, et al., 2018*) Therefore, this study processes the data in the frequency domain to obtain velocity information while analyzing the primary sources of vibration at each measurement point.

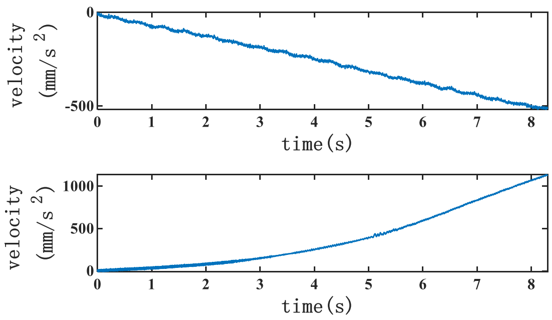

Fig. 6 - Velocity variation chart obtained by integrating untreated time-domain data from some measurement points

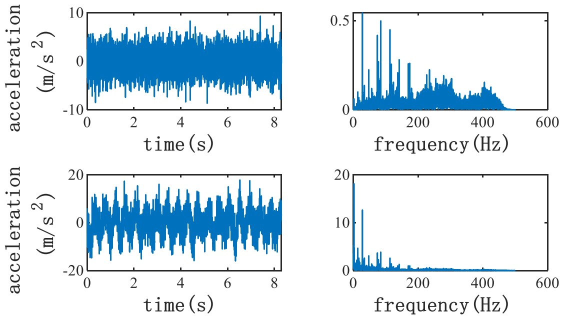

Fig. 7 - Time-domain and frequency-domain feature plot for measurement point 1

The Fast Fourier Transform (FFT) is used to convert the time-domain discrete signals collected by the accelerometers into the frequency domain. FFT is a computationally efficient method that simplifies the Discrete Fourier Transform (DFT) for faster calculations. While they are fundamentally equivalent, both methods perform the transformation of the time-domain signal as described in the following equation:

$$X(k)=\sum_{n=0}^{N-1} x(n)e^{-j\frac{2\pi}{N}kn}(k\text{=0,1,2…}N\text{-1}) \tag{2}$$

In the context of FFT or DFT transformation, the symbols can be defined as follows:

- $X(k)$: Represents the frequency-domain signal in its complex form after FFT or DFT transformation.
- $x(n)$: Represents the discrete time-domain signal.
- $e^{-j\frac{2\pi}{N}kn}$: Describes the unit circle in the frequency domain, as defined by Euler's formula.
- k: Represents the frequency-domain signal sequence.
- N: Represents the total number of data points in the time-domain signal.
- j: Represents the imaginary unit.

The relationship between the time-domain integral of a digital signal and its corresponding representation in the frequency domain can be expressed by the following equation:

$$\mathcal{F}\left[\int_{-\infty}^{t} f(\tau)d\tau\right]=\frac{F(\omega)}{j\omega}+\pi F(0)\delta(\omega) \tag{3}$$

In the equation provided, the following symbols represent specific concepts:

- $\mathcal{F}$: Represents the Fourier transform.
- $\int_{-\infty}^{t} f(\tau)d\tau$: Indicates the time-domain integration of the digital signal.
- $F(\omega)$: Represents the frequency-domain value of the digital signal.
- $F(0)$: Represents the DC component.
- $\delta(\omega)$: Denotes the unit impulse function, an idealized narrow pulse with an area equal to 1.
- t: Represents the maximum time point of the selected time interval.
- ω: Represents the frequency-domain variable.

For the discrete data collected during the experiment, $F(\omega)$ = $X(k)$ and $j\omega$ = jk.

In general, the DC component is the primary factor causing trends in integration results; therefore, $F(0)$ is set to 0. To obtain the time-domain integral of the digital signal, it is sufficient to divide its frequency-domain data by $j\omega$ f and then perform the inverse Fourier transform (IFT).

The process involves using the Fast Fourier Transform (FFT) to convert the acceleration signals from each measurement point into frequency-domain form. After processing the data in the frequency domain, the velocity is obtained through the inverse Fourier transform.

For example, the time-frequency characteristics of the acceleration and velocity at measurement point 1 are illustrated in Figure 7, demonstrating how the transformation and processing effectively capture the vibrational behavior of the chassis.

Analysis of Vibration Velocity at Measurement Points

After performing frequency domain integration on the vibration acceleration data collected from various measurement points of the engine under low-speed conditions, it was found that the vibration velocity does not exhibit a periodic variation exceeding 2 seconds in the time domain. To improve computational efficiency while ensuring the completeness of frequency domain information, acceleration data collected over 2 seconds at mid to high engine speeds, characterized by shorter periods, were selected for processing. It is assumed that this data contains velocity and acceleration information encompassing more than one cycle, thereby excluding frequency domain data below 0.5 Hz. The frequency characteristics of the first three modes of vibration velocity in different directions at various engine speeds (high, medium, and low) for all measurement points are presented in Table 3.

Due to the resolution limitations of frequency domain data and the fact that the engine speed remains at a specific value near the preset rotation speed, the experimentally measured vibration frequencies of excitation sources exhibit minor deviations from their theoretical values. As indicated in Tables 1 and 3, under low-speed conditions, the vibrations at measurement points on the chassis frame are influenced comparably by excitations from engine cylinder ignition, cutter drive shaft, and vibrating sieve, with their respective frequencies contributing comparably to the observed vibration spectra. However, at medium and high rotation speeds, except for measurement points 5 and 6 near the engine - which predominantly exhibit a dominant vibration frequency of 91.8 Hz in the z-direction (closely matching the engine excitation frequency) - other measurement points primarily demonstrate vibration frequencies adjacent to those generated by the vibrating sieve and cutter drive shaft. This characteristic is particularly pronounced in the x- and y-directions. These findings suggest that the reciprocating motions of the header and vibrating sieve progressively surpass engine-induced excitations as rotation speed increases, ultimately emerging as the predominant excitation sources affecting the chassis frame. This phenomenon highlights the speed-dependent evolution of excitation dominance in harvester dynamic responses.

Table 3

Frequencies of the First Three Orders of Vibration Velocity

Measurement Points	Fundamental Frequency/Hz (Velocity /m•s^{-1})								
	Low Speed			Medium Speed			High Speed		
	x	y	z	x	y	z	x	y	z
Measurement Points 1	28.32 (18.1)	28.81 (3.7)	28.32 (18.2)	4.88 (77.9)	4.88 (41.2)	3.91 (63.8)	7.32 (150.0)	8.79 (75.5)	7.32 (80.5)
Measurement Points 2	28.32 (17.8)	2.93 (4.9)	2.44 (17.1)	4.88 (78.5)	4.88 (11)	3.91 (57.5)	7.32 (151.5)	1.46 (60.2)	7.32 (97.8)
Measurement Points 3	2.44 (17.8)	28.81 (2.7)	47.85 (19.1)	4.88 (83.6)	4.88 (26.1)	3.91 (66.8)	7.32 (156.8)	8.79 (56.7)	7.32 (154.5)
Measurement Points 4	3.42 (4.8)	28.32 (5.2)	28.32 (40.3)	4.88 (13.9)	4.39 (28.7)	30.27 (22.2)	8.30 (55.9)	8.79 (69.8)	7.32 (45.1)
Measurement Points 5	3.42 (2.6)	56.64 (4.0)	28.32 (14.6)	30.27 (15.6)	4.39 (14.4)	30.27 (15.7)	8.30 (69.4)	8.79 (12.3)	91.80 (43.5)
Measurement Points 6	2.44 (17.4)	2.44 (9.3)	2.44 (34.7)	4.88 (35.5)	4.39 (24.4)	3.91 (30.1)	8.30 (105.5)	8.79 (48.0)	7.32 (62.5)
Measurement Points 7	28.32 (6.8)	28.32 (3.2)	1.95 (5.7)	28.32 (6.8)	4.39 (16.7)	28.32 (4.8)	4.39 (17.5)	8.79 (30.8)	3.91 (15.3)
Measurement Points 8	28.32 (17.0)	2.93 (1.3)	28.32 (9.2)	3.91 (21.1)	4.88 (8.3)	28.81 (8.9)	8.30 (49.9)	8.79 (4.0)	7.32 (54.7)
Measurement Points 9	47.85 (6.6)	28.32 (2.9)	1.95 (24.5)	4.88 (13.3)	3.91 (31.3)	3.91 (15.0)	8.30 (89.5)	7.32 (69.9)	7.32 (32.4)
Measurement Points 10	47.85 (12.5)	1.95 (7.7)	84.96 (8.4)	4.88 (13.3)	3.42 (5.2)	3.91 (10.1)	8.30 (76.4)	1.46 (126.1)	7.32 (41.7)
Measurement Points 11	2.93 (14.9)	28.32 (4.2)	28.32 (43.9)	3.91 (18.3)	4.88 (16.7)	29.30 (19.9)	8.30 (43.2)	7.32 (38.8)	34.67 (48.8)
Measurement Points 12	2.44 (13.6)	28.32 (2.6)	1.46 (7.8)	4.88 (20.9)	4.88 (21.9)	3.91 (19.7)	8.30 (97.7)	7.32 (46.3)	7.32 (42.3)

At medium and high speeds, the reciprocating motion of the cutting platform and vibrating screen increasingly affects the chassis frame as the speed rises. Only measurement points 5 and 6, close to the engine, exhibit a principal vibration frequency of 91.8 Hz in the z-direction at high speeds, closely aligning with the engine excitation frequency. Consequently, in 30 out of the 36 data sets from the 12 measurement points, the primary vibration frequencies align more closely with the excitation frequencies from the vibrating screen and cutting platform, indicating a shift in the primary excitation source from the engine to these components.
Since the cutting platform and vibrating screen are located on the left side between the chassis frames, their reciprocating motions generate inertial forces that also apply torsional moments to the chassis frame. This could explain why measurement points in the x and y directions are significantly influenced by the cutting platform and vibrating screen.

The root mean square (RMS) values of the vibration velocities for each measurement point were calculated and are presented in Figure 8. Overall, at low engine speeds, the vibration velocities in the x, y, and z directions at most measurement points are close to the boundaries of vibration levels A and B. At medium speeds, the vibration intensities at most points do not significantly change from low speeds; however, measurement points 1, 2, and 3—located at the rear of the chassis frame and far from the support structure—exhibit significantly higher vibration intensities across all three testing directions, reaching vibration levels C and D.

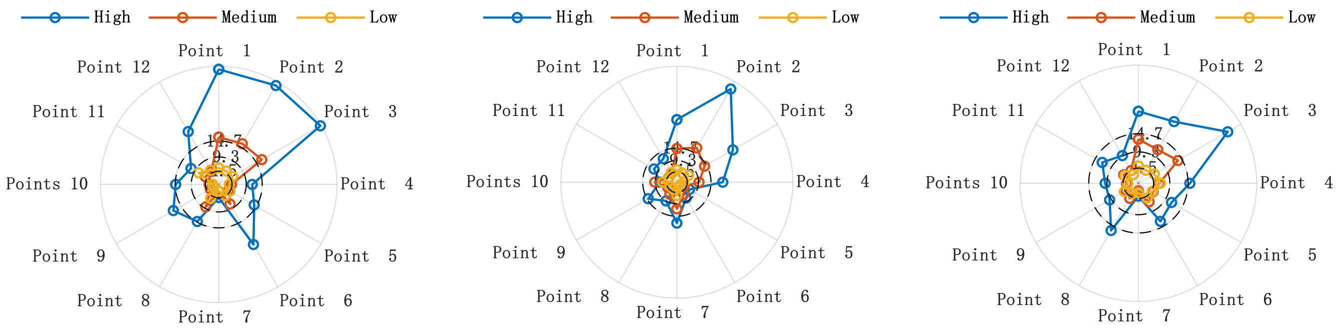

(a)The RMS of the vibration velocity at each measurement point in the x direction.

(b) The RMS of the vibration velocity at each measurement point in the y direction.

(c) The RMS of the vibration velocity at each measurement point in the z direction.

Fig. 8 - The vibration status of each measurement point

At high speeds, the vibration levels at all measurement points increase noticeably. Points that already displayed higher vibrations at medium engine speeds exhibit even greater intensities at high speeds. This suggests that, at medium engine speeds, the structural strength of the chassis frame, particularly away from the support locations, is beginning to fail under the demands of excitation from the vibrating screen and cutting platform, and this phenomenon becomes more pronounced at high engine speeds.

STRUCTURAL OPTIMIZATION OF THE COMBINE HARVESTER

To reduce the vibrations in the chassis frame of the combine harvester, improvements are made from two aspects: enhancing the structural strength of the frame and reducing excitation. First, structural reinforcements are applied to the regions at the rear of the chassis frame, specifically near measurement points 1, 2, and 3, which are far from the support points, as illustrated in Figure 9.

To decrease the excitation experienced by the chassis frame, vibration-damping pads are added at the connections between the cutting platform's hydraulic cylinders and the vibrating screen's drive shaft bearings. Additionally, given the inherent characteristics of the vibrating screen, achieving complete balance while ensuring the proper operation of other components is unrealistic. Instead, measures can be taken to reduce the area of the overall center of mass movement trajectory of the vibrating screen, thereby lowering its excitation on the chassis frame (*Wang et al., 2012; Zhang et al., 2012; Li et al., 2016*).

Considering the principles of dynamic balance and the structural features of the vibrating screen and its nearby components, the decision was made to modify the center of mass of the vibrating screen's drive pulley and add eight cast iron counterweights, as depicted in Figure 10. A three-dimensional model of the vibrating screen was created, and simulations of its motion characteristics were conducted using Adams software to calculate the trajectory of the vibrating screen system's center of mass. The changes in the center of mass before and after implementing the dynamic balance design are shown in Figure 11.

After adding the counterweights, the area of the center of mass movement trajectory for the vibrating screen system was reduced, and it also moved closer to the coordinates of the drive shaft center (-1000, 0). Theoretically, this adjustment successfully weakens the inertial forces caused by the movement of the vibrating screen's center of mass.

Following these structural modifications, the vibration testing of the chassis frame was conducted again using the previously described methods. The results indicated that the vibration intensities at various measurement points were reduced to varying degrees. For example, at the more vibrationally intense measurement points 1, 2, and 3, the changes in vibration intensity at different engine speeds are summarized in Table 4.

At low engine speeds, the excitation experienced by the chassis frame is relatively low, resulting in minimal changes in vibration intensity compared to the mid and high-speed conditions. As the engine speed increases, the excitation on the chassis frame rises continuously, highlighting the advantages of the optimized structure. At high engine speeds, the average vibration intensity at the three measurement points decreased by 34.57% in different directions. Notably, the vibration velocity at measurement point 3 in the x-direction decreased from 42.67 mm·s^{-2} to 11.51 mm·s^{-2}, shifting the vibration level from D to C, indicating a significant reduction in vibration intensity.

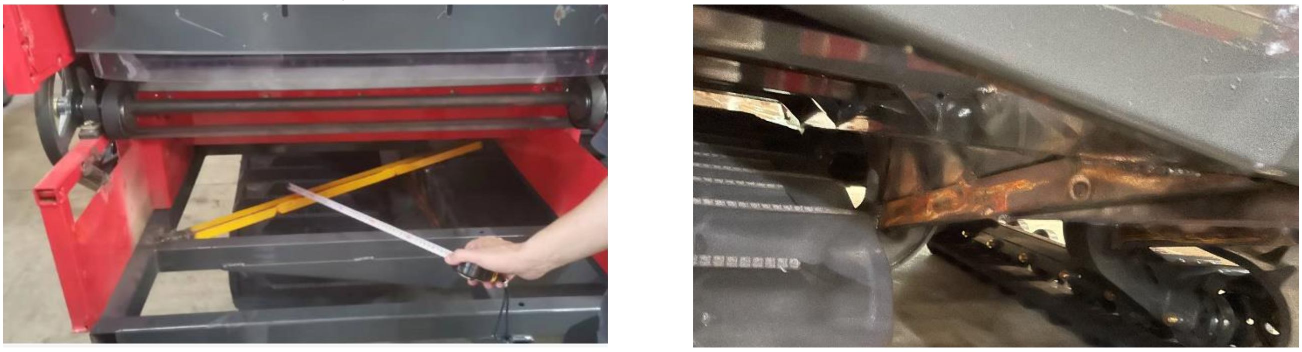

(a) Enhancement of horizontal structural integrity. (b) Enhancement of vertical structural integrity.

Fig. 9 - Partial structural reinforcement locations

Fig. 10 - Vibration sieve motion balance design

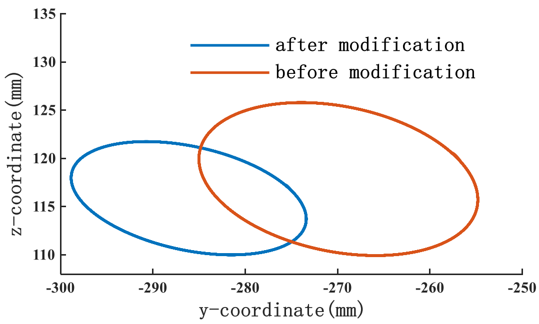

Fig. 11 - Motion trajectory of the centroid of the vibration sieve

Table 4

The root mean square of vibration velocity for selected measurement points on the chassis frame before and after structural optimization

Measurement Points		Low Speed / mm•s^{-2}			Medium Speed / mm•s^{-2}			High Speed / mm•s^{-2}		
		x	y	z	x	y	z	x	y	z
Measurement Points 1	before modification	6.01	6.02	5.36	17.88	15.20	14.40	41.94	30.51	21.43
	after modification	4.11	5.68	7.19	9.91	11.88	10.12	20.13	18.83	19.84
Measurement Points 2	before modification	5.59	4.76	4.85	17.89	7.65	12.40	41.60	17.20	21.46
	after modification	4.17	3.33	6.66	9.51	5.40	9.24	19.52	22.17	16.95
Measurement Points 3	before modification	5.82	4.46	6.32	18.97	14.64	14.51	42.67	29.40	31.84
	after modification	3.15	5.09	5.03	5.15	6.36	11.90	11.51	13.49	18.77

CONCLUSIONS

Static Analysis: Finite element analysis of the combine harvester's chassis frame revealed that the areas farthest from the support structure, particularly around the vibrating screen and threshing cylinder, experienced the greatest deformation. The maximum stress and strain were located near the support points, indicating these are relatively weak regions of the frame.

Vibration Velocity Measurement: Frequency-domain processing of the measured vibration acceleration data successfully provided the vibration velocities at various measurement points. According to the international standard ISO 20816, the original vibration levels of all points in the chassis frame were classified as the highest D level under high engine speeds.

Influence of Components: An analysis of the principal vibration frequencies at different engine speeds revealed that the impact of the vibrating screen and cutting platform on the chassis frame increased with engine speed. At high speeds, 30 out of 36 sets of data showed principal frequencies closely aligned with the excitation frequencies of the vibrating screen and cutting platform drive shafts.

Mitigation Measures: To reduce vibration intensity at various measurement points, enhancements to the chassis structure were implemented, vibration-damping pads were added at the connections between the excitation sources and the chassis, and the area of the vibrating screen's center of mass movement trajectory was minimized. Testing indicated an average vibration intensity reduction of 34.57% at the three previously most affected measurement points under high engine speeds.

Although the structural enhancements have successfully diminished the vibration intensity, the levels remain relatively high. Further research is necessary to analyze the effects of other factors, such as the center of mass of the combine harvester and support points on the chassis frame vibrations.

ACKNOWLEDGEMENT

This research was funded by the National Natural Science Foundation of China (32171911) and the National Key Research and Development Program of China (2021YFD2000503).

REFERENCES

[1] Biriș S.Șt, Constantin A-M., Anghelache D., Găgeanu I., Cujbescu D., Nenciu F., Voicea I., Matei Gh., Popa L-D., Duțu M.F., Ungureanu N., Żelaziński T., Perișoară L., Fodorean G. (2022). Considerations regarding the vibrations transmitted to the operator by an axial flow harvester combine, *INMATEH – Agricultural Engineering*, Vol. 68 (3), pp. 747-756, https://doi.org/10.35633/inmateh-68-74

[2] Chen S.R., Zhou Y P, Tang Z, Lu S N. (2020). Modal vibration response of rice combine harvester frame under multi-source excitation [J]. *Biosystems Engineering*, Vol. 194, pp. 177-195. https://doi.org/10.1016/j.biosystemseng.2020.04.002

[3] Dimitriadis C., Kateris D., Xyradakis P., Gialama A., Gialamas T. (2023). Vibration assessment of tractor driver based on vibration signals, *INMATEH – Agricultural Engineering*, Vol.71 (3), pp.776-784, https://doi.org/10.35633/inmateh-71-68

[4] Ding H.T., Chen S.R., Zhou W.W., Liang R.Z. (2022). A Mechanism analysis of combine harvester's vibration characteristics under feeding interference（喂入量扰动下联合收获机振动特性机理研究）[J]. *Transactions of Chinese Society for Agricultural Machinery*, Vol.53 (S2), pp.20-27+51. https://doi.org/10.6041/j.issn.1000-1298.2022.S2.003

[5] Gao Z.P., Xu L.Z., Li Y.M., Wang Y.D., Sun P.P. (2017). Vibration measure and analysis of crawler-type rice and wheat combine harvester in field harvesting condition (履带式稻麦联合收获机田间收获工况下振动测试与分析) [J]. *Transactions of the Chinese Society of Agricultural Engineering*, Vol.33(20), pp.48-55. https://doi.org/10.11975/j.issn.1002-6819.2017.20.006

[6] Hu Y.M., Zhou Y.J., Zhu H., Chen X.L., Sun J.M., Pi Y.J. (2015). Integration algorithm based on trend-control of error in frequency domai (基于趋势项误差控制的频域积分算法研究与应用) [J]. *Journal of Vibration and Shock*, Vol. 34 (02), pp. 171-175. https://doi.org/10.13465/j.cnki.jvs.2015.02.030

[7] Jiang Y.J., Liao Y.T., Qin C., Guan Z.H., Liao Q.X. (2017). Vibration Analysis and Improvement for frame of 4SY-2.9 typed rape windrow (4SY-2. 9 型油菜割晒机机架振动分析及改进) [J]. *Transactions of the Chinese Society of Agricultural Engineering*, Vol.33 (09), pp.53-60. https://doi.org/10.11975/j.issn.1002-6819.2017.09.007

[8] Karagiovanidis M., Pantazi X.E., Papamichail D., Fragos V. (2023). Early Detection of Cavitation in Centrifugal Pumps Using Low-Cost Vibration and Sound Sensors. [J]. *Agriculture*., Vol.13 (8), 1544, https://doi.org/10.3390/agriculture13081544

[9] Li G., Wang C., Li Y.C., Fang M.H. (2016). Investigation on Inertial Force Balancing of Slider -crank Type Cleaning Sieve (曲柄滑块式清选筛机构惯性力平衡研究) [J]. *Journal of Agricultural Mechanization Research*, Vol. 38 (08), pp. 24-30+35. https://doi.org/10.13427/j.cnki.njyi.2016.08.005

[10] Li J.Y., Li X.Q., Li Y.D., Zhang Y.X.M., Yang X.K., Xu P.X. (2023). A new method of tractor engine state identification based on vibration characteristics [J]. *Processes*, Vol.11 (2), pp.303. https://doi.org/10.3390/pr11020303

[11] Ma L.N., Wei J.Y., Huang X.M., Song W.Y., Zhan G.C. (2020). Analysis of Harvesting Losses of Rapeseed Caused by Vibration of Combine Harvester Header during Field Operation (油菜联合收获机割台振动对田间收获落粒影响分析). [J]. *Transactions of Chinese Society for Agricultural Machinery*, Vol. 51 (S2), pp. 134-138+201. https://doi.org/10.6041/j.issn.1000-1298.2020.S2.016

[12] Marin, E., Cârdei, P., Vlăduţ, V., Biriş, S.Şt., Ungureanu, N., Bungescu, S.T., Voicea, I., Cujbescu, D., Găgeanu, I., Popa, L-D., Isticioaia, S., Matei, Gh., Boruz, S., Teliban, G., Radu, C., Kabas, O., Caba, I., Maciej, J. (2024). Research on the influence of the main vibration-generating components in grain harvesters on the operator's comfort, *INMATEH Agricultural Engineering*, Vol. 74 (3), pp. 808-823, https://doi.org/10.35633/inmateh-74-71

[13] Li Wang, Li Shou, Lv Dianji, Ekhlo Ghay (2021). Multi-sensor signal acquisition and data processing analysis of combine harvester, *INMATEH – Agricultural Engineering*, Vol.63 (1), pp.335-344, https://doi.org/10.35633/inmateh-63-34

[14] Noh J.H., Kim P., Yoon Y.J. (2024). Competitive advantages of a bistable vibration isolator: Cut-off frequency and operational safety near harmful resonance [J]. *Journal of Sound and Vibration*, Vol. 570 (03). https://doi.org/10.1016/j.jsv.2023.118004

[15] Pang J., Li Y.M., Ji J.T., Xv L.Z. (2019). Vibration excitation identification and control of the cutter of a combine harvester using triaxial accelerometers and partial coherence sorting [J]. *Biosystems Engineering*, Vol. 185, pp. 25- 34. https://doi.org/10.1016/j.biosystemseng.2019.02.013

[16] Rabbani M.A., Tsujimoto T., Mitsuoka M., Inoue E., Okayasu T., (2011). Prediction of the vibration characteristics of half-track tractor considering a three-dimensional dynamic model [J]. *Biosystems Engineering*, Vol. 110 (2), pp.178-188. https://doi.org/10.1016/j.biosystemseng.2011.07.013.

[17] Sun Z., Wang L., Pan Z. (2014). Analyses of vibration characteristics of power fan for the 4ztl-1800 pneumatic conveying combine stripper harvester [J]. *Transactions of the ASABE*, Vol. 57 (3), pp. 693-699. https://doi.org/10.13031/trans.57.10317

[18] Tang Z., Zhang B., Wang M.L., Zhang H.T. (2021). Damping behaviour of a prestressed composite beam designed for the thresher of a combine harvester [J]. *Biosystems Engineering*, Vol. 204, pp.130-146. https://doi.org/10.1016/j.biosystemseng.2021.01.020

[19] Vlăduţ V., Biriş S.Şt., Paraschiv G., Ungureanu N., Bungescu S.T., Voicea I., Cujbescu D., Găgeanu, I., Laza E., Popa L-D., Matei Gh., Atanasov At. (2023). Considerations regarding the effects of shocks and vibrations on operators of self-propelled agricultural equipment, *INMATEH –Agricultural Engineering*, Vol. 71 (3), pp. 843-856, https://doi.org/10.35633/inmateh-71-74

[20] Wang L., Li S., Lv D., Ekhlo G. (2021). Ulti-sensor signal acquisition and data processing analysis of combine harvester, *INMATEH – Agricultural Engineering*, Vol. 63(1), pp.335-344, https://doi.org/10.35633/inmateh-63-34

[21] Wang Q., Luo K., Yang J., Jiang L.B. (2012). Research on inertial force balance of a shaker in a combine harvester (联合收割机振动筛机构惯性力平衡的研究) [J]. *Mechanical Research & Application*, No.06, pp.36-39.

[22] Wei C.C., Xu L.Z., Wang J.T., Li Y.M. (2018). Inertial force balance and ADAMS simulation of the oscillating sieve and return pan of a rice combine harvester [J]. *International Journal of Agricultural and Biological Engineering*, Vol.11 (01), pp. 129-137. https://doi.org/10.25165/j.ijabe.20181101.2978

[23] Wu L.M., Bi Y.H., Wu B., Lei J.L., Shen L.Z. (2020). Analysis of influence of piston secondary motion on vibration and noise of non-road high pressure common rail diesel engine (活塞二阶运动对非道路高压共轨柴油机振动及噪声影响分析) [J]. *Journal of Vibration and Shock*, Vol. 39(11), pp. 193-200. https://doi.org/10.13465/j.cnki.jvs.2020.11.026

[24] Xie H.R., Jin C.Q., Yin X., Qian Z.J., Teng Y.J., Yv C.X. (2019). Vibration Measurement and Analysis of Tracked Soybean Combine Harvester（履带式大豆联合收获机振动测试与分析）[J]. *Journal of Agricultural Mechanization Research*, Vol. 41(08), pp. 158-163+174. https://doi.org/10.13427/j.cnki.njyi.2019.08.027

[25] Yao Y.C., Song Z.H., Du Y.F., Zhao X.Y., Mao E.R., Liu F. (2017). Analysis of vibration characteristics and its major influenced factors of header for corn combine harvesting machine (玉米收获机割台振动特性及其主要影响因素分析) [J]. *Transactions of the Chinese Society of Agricultural Engineering*, Vol. 33 (13), pp.40-49. https://doi.org/10.11975/j.issn.1002-6819.2017.13.006

[26] Zhang H.T. (2012). Research on the Kinematics and inertial force balance of the vibrating screen (振动筛机构的运动分析和惯性力平衡研究）[D]. Cheng Du: School of Mechanical Engineering, Xihua University.

[27] Zhang H.T. (2021). Research on Disturbed Vibration Characteristics of Combine Harvester Threshing Cylinder and Vibration Isolation Method (水稻联合收获机脱粒滚筒受扰振动特性及隔振方法研究), [D]. College of Agricultural Engineering, Zhen jiang: Jiangsu University. https://doi.org/10.27170/d.cnki.gjsuu.2020.000176

[28] Zhang L.J., Zhou H., Yu Z.P., Jin X.X. (2001). Research on Control of Car Interior Noise due to Engine Vibration (发动机振动引起的车内噪声控制研究) [J]. *Journal of Vibration, Measurement & Diagnosis*, No. 01, pp. 61-66+76. https://doi.org/10.16450/j.cnki.issn.1004-6801.2001.01.012

[29] Zhang M.J., Jin J.F., Chen Y.Y., Chen T.K. (2023). Vibration symmetry characteristics of wheeled tractor structure (轮式拖拉机对称结构的振动特性) [J]. *Journal of Jilin University (Engineering and Technology Edition)*, Vol. 53 (07), pp. 2136-2142. https://doi.org/10.13229/j.cnki.jdxbgxb.20220313

[30] Zhou Y., Wang X., Hou Y., Que H.B., Guo R.B., Lin X.H., Jin S.Q., Wu C.P. (2023). Test study on vibration behavior and bearing load characteristics of high-speed train gearbox under internal excitation(内部激励下高速列车齿轮箱振动行为及轴承载荷特性实验研究) [J]. *Journal of Vibration and Shock*, Vol. 42 (13), pp. 242-250. https://doi.org/10.13465/j.cnki.jvs.2023.13.029